Finite Elements in Analysis and Design 139 (2018) 35–48

Contents lists available at ScienceDirect

Finite Elements in Analysis and Design

journal homepage: www.elsevier.com/locate/finel

Incremental volumetric and Dual Kriging remapping methods

C. Miguel [a,*], D.M. Neto [a], M.C. Oliveira [a], J.L. Alves [b], L.F. Menezes [a]

[a] CEMMPRE, Department of Mechanical Engineering, University of Coimbra, Polo II, Rua Luís Reis Santos, Pinhal de Marrocos, 3030-788, Coimbra, Portugal
[b] CMEMS, Microelectromechanical Systems Research Unit, University of Minho, Campus de Azurém, 4800-058, Guimarães, Portugal

ARTICLE INFO

Keywords:
Finite Element Method
Remapping
Dual Kriging
Trimming
Hexahedral finite elements
DD3TRIM

ABSTRACT

The transfer of variables between distinct spatial domains is a problem shared by many research fields. Among other applications, it may be required for visualization purposes or for intermediate analysis of a process. In any case, two important factors must be considered: accuracy and computational performance. The accuracy becomes more important when the results have an impact on the subsequent stages of the process' analysis, as it could lead to incorrect results. The computational performance is a permanent requirement due to the ever-increasing complexity of the analysed processes. The aim of this work is to present a new remapping method, based on Dual Kriging interpolation, developed to enable accurate and efficient variable transfer operations between two different domains, discretized with hexahedral finite elements. Two strategies are proposed, which take into account different selections of interpolation points and are based on specific Finite Element Method features. They are compared with the Incremental Volumetric Remapping method in two remapping examples, one of which includes a trimming operation, highlighting their advantages and limitations. The results show that the Dual Kriging remapping method, combined with a 2D selection strategy for the donor points, can contribute to increase the accuracy of the state variables remapping operation, particularly when they present a strong gradient along the stacking direction.

1. Introduction

The Finite Element Method (FEM) emerged in the sixties, enabling the solution of problems that could not be solved analytically [1,2]. Whatever the application field, FEM requires the partition of the spatial domain into finite elements, which define the mesh that approximates the original domain. The type of finite elements used depends on the application field or problem (e.g. Ref. [3]), and varies between 1D, 2D, and 3D, using interpolation functions of different degrees. The linear isoparametric hexahedral and tetrahedral finite elements are commonly used in 3D simulations, adopting different mesh topologies.

The solution of nonlinear problems also requires the division of the temporal domain to take into account time dependant variables related to geometrical, material or boundary conditions nonlinearities [4]. Typically, resorting to more divisions – spatial and temporal – increases the accuracy of the numerical results, at the cost of the computational performance (e.g. Refs. [5,6]). Therefore, it is always necessary to find the best equilibrium between results accuracy and computational effort. In terms of spatial discretization, the definition of zones with different mesh sizes can be performed either in the pre-processing stage or during the numerical simulation. The definition of different zones in the pre-processing is usually carried out manually, which contributes to an increase of the time required for this stage. On the other hand, during the numerical simulation, the definition of different zones requires the application of adaptive mesh refinement/remeshing algorithms (e.g. Refs. [7,8]), in several temporal increments. In fact, adaptive mesh refinement algorithms are commonly used to overcome problems of excessive distortion/deformation of the finite elements, which occur in different forming processes [7,9], such as forging [10,11] and sheet metal forming [12]. The adaptive mesh refinement is usually performed by one of three methods: *p*-adaptive (change of the interpolation degree), *h*-adaptive (change of the element size), *r*-adaptive (change of the nodes' location); or by a combination of them [8]. The improvement of these methods is an up to date research topic in computational mechanics [13], since small improvements have a considerable impact on computational performance, as they can be applied several times during the simulation.

The adoption of adaptive mesh refinement algorithms involves a remapping step, i.e. the transfer of variables between different spatial discretizations [14,15], which can present a strong influence on the accuracy of the results and computational efficiency. Nonetheless, in some

* Corresponding author.
E-mail addresses: carlosmiguelpapers@gmail.com (C. Miguel), diogo.neto@dem.uc.pt (D.M. Neto), marta.oliveira@dem.uc.pt (M.C. Oliveira), jlalves@dem.uminho.pt (J.L. Alves), luis.menezes@dem.uc.pt (L.F. Menezes).

https://doi.org/10.1016/j.finel.2017.10.005
Received 20 April 2017; Received in revised form 12 October 2017; Accepted 24 October 2017
Available online 8 November 2017

cases the zone to be remapped can be narrow, as in the numerical analysis of trimming operations involved in some multi-stage forming processes. Typically, these operations consist in the geometrical trimming of the FE mesh (e.g. Ref. [10]), which is also the focus of this work. Thus, after each trimming operation, it is also necessary to perform a remapping procedure for the numerical variables involved in the subsequent forming steps. In this case, the impact of the selected remapping method on the computational efficiency is reduced, but its accuracy can have a strong influence on the results of the subsequent numerical simulation. When using the FEM, it can be necessary to transfer the nodal variables (primary unknowns), such as forces and displacements; and the state variables (secondary unknowns), which are evaluated in the integration points (typically Gauss points), such as the stress and strain state. The former are usually continuous while the latter are discontinuous (e.g. Ref. [7]). The current work is mainly focused on the transfer of state variables, evaluated in the integration points.

Jiao and Health [14], divide the remapping methods into four major groups. The first group refers to pointwise interpolation and extrapolation methods, such that the variables are transferred using a function that interpolates/extrapolates the variables from the donor (old) mesh to the target (new), in one or more stages. The pointwise interpolation can be categorized into two types: (i) use of the same shape function as the one for the donor mesh (sometimes referred to as consistent interpolation or inverse isoparametric mapping (e.g. Refs. [16,17])) and (ii) use of basis functions of higher order than the one of the donor basis. According to Baptista [18], taking into account the mathematical characteristics of these methods, this group can also include the ones based on the application of the moving least squares [15,19] and the Superconvergent Patch Recovery methods, developed by Zienkiewicz and Zhu [20]. The second group refers to Area/Volume weighted averaging methods (also referred as Finite Volume Transfer Method in Ref. [11]), which uses a transfer function that is evaluated based on the area/volume of intersection between the donor and the target FE. The corresponding areas/volumes act as a weighting factor defining the contribution of each donor element to the target one (e.g. Refs. [21,22]). The third group refers to Mortar element methods, which are general techniques for projecting data at interfaces between two or more non-conforming subdomains [11]. From a mathematical point of view, this method consists in the minimization of a weighted residual, where the weight functions are usually chosen from the space spanned by the basis functions of the mortar side [23]. The last group refers to specialized methods, which are designed for specific applications and do not fall directly into the above categories, but frequently are variants or combinations of them. This fourth group includes the direct allocation to the target point of the closest donor point [24], the use of different methods according to the type of variable [9], and adaptations of the interpolation/extrapolation and area/volume weighted averaging methods; by including constraints [25]; and/or considering specific features of the application domain or problem [26,27].

The accurate transfer of variables between different spatial discretizations is imperative, independently of the remapping method adopted. Moreover, its computational performance is particularly important when the procedure is performed several times, while the error is accumulated to the subsequent stages (e.g. Refs. [7,11]). In fact, the remapping operation can introduce errors due to the approximations used to estimate the values for the target mesh. In order to try to control and minimize the unavoidable errors when performing remapping operations, several authors [11,14,15,17,25] point out some desirable characteristics. The method should be self-consistent such that when the target and the donor point are coincident, the transfer remapping function reduces to the identity operator (null error). The interpolation/extrapolation methods that resort to the donor shape functions cannot guarantee, *a priori*, this condition [15]. On the contrary, Area/Volume weighted averaging methods automatically verify this self-consistency condition. The method should also guarantee the locality, i.e. the remapped value in a target point should only be affected by the variables of the donor mesh in a region of influence. This assures the preservation of discontinuities, related with material or geometric interfaces, which must also be present in the remapped mesh. However, due to the discrete and approximated natured of the remapping operations, it is always expected some degradation (smoothing) of the variable value when severe gradients are present. Nonetheless, the smoothing should be minimized in order to preserve, as accurately as possible, the gradients of the donor mesh. On the other hand, the remapping method can also lead to spurious local extreme values, which are non-physical and result in the degradation of the numerical simulation result. Accordingly, the remapping algorithm should allow for the inclusion of some constraints, such as consistency of equilibrium or motion equations [25], consistency between the displacement field and the stress state or boundary conditions [17].

In order to take advantage of the characteristics of these applications, several specialized remapping methods have been proposed, in order to find the best equilibrium between accuracy and computational performance. One example is the application of the moving least squares method, proposed by Rashid [15], based on a transfer function. It attempts to force the equality between the variable field in a volumetric domain of the donor and of the target mesh, assuming that each donor integration point has constant state variables in a predefined region. Jiao and Heath [14] present a general method, named Common Refinement, which is based on the intersection of the donor and target mesh in order to define a third mesh, used as an auxiliary for the transfer procedure. The main advantage of this method is that it allows the accurate integration of the transfer function, which depends on the shape functions of the target and donor meshes. However, it requires a robust and expeditious algorithm for mesh intersection, which is considerably challenging to attain when working with solid hexahedral finite elements. In this context, also the Incremental Volumetric Remapping (IVR) method was developed and applied, specifically for the transfer of variables between meshes composed of linear isoparametric hexahedrons [18]. This volume-weighted averaging method assumes that each donor integration point has constant state variables in a predefined region [15]. Being a volume-weighted averaging method, some of the desirable characteristics are inherently verified (self-consistency, locality, and inexistence of spurious local extrema values), which makes it particularly interesting for FEM analysis.

The IVR method has been previously implemented in the in-house code DD3TRIM [18], which has been specifically developed for performing geometrical trimming operations of 3D meshes, composed by linear isoparametric hexahedrons. In sheet metal forming operations, this type of elements is typically used with a selective reduced integration scheme [28]. Thus, for each element, the state variables are evaluated in eight different integration points, also called Gauss Points (GPs), since their spatial positions in the finite element's natural coordinates are defined by the Gauss Quadrature Rule [4]. The accurate transfer of the state variables is fundamental to enable the proper numerical simulation of forming process, involving trimming operations.

In previous works [18,29,30], the performance of the IVR algorithm was compared with the classic interpolation/extrapolation method, using a transfer function based on the shape function of the linear isoparametric elements. Additionally, it was compared with the moving least square interpolation method, using an exponential based curve as weight function [18,29]. The results show that the error associated to the IVR is lower when compared to these other two methods, particularly when increasing the number of consecutive remapping operations. In addition, the IVR method is robust in critical situations, such as poor geometrical definition of the mesh domain boundaries, where some nodes of the target mesh fall outside the donor mesh. However, concerning the computational cost, it was observed that the classical extrapolation/interpolation method was clearly the fastest, while the IVR method and the one based on moving least squares interpolation presented similar computational costs [18,29].

This study presents a new remapping method dedicated to finite

element meshes composed by isoparametric hexahedrons, which uses the Dual Kriging method. This interpolation method is known for being simple while incurring a small computational cost in the interpolation of space-dependent variables [31]. The Incremental Volumetric method is briefly described in the following section, since it will be used as reference to evaluate the performance of the Dual Kriging remapping strategies proposed. The Dual Kriging interpolation method is described in the same section, as well as the strategies adopted to select the set of donor GPs. These strategies were implemented in the in-house code DD3TRIM, allowing the comparison in terms of accuracy and computational efficiency. Two examples are selected to perform the comparison between the two remapping methods: the first comprises an analytical function distribution, which is mapped between two different finite element meshes, while the second example covers a trimming operation performed on a metallic sheet.

2. Remapping methods

2.1. Incremental Volumetric Remapping (IVR) method

The Incremental Volumetric method is established assuming that the variables values in the region of a Gauss volume (an eight part of the standard brick element) are equal to the state variable quantity placed in the correspondent Gauss point [15]. The subdivision of a finite element into eight Gauss volumes is presented in Fig. 1. Accordingly, the variable value assigned to a given Gauss point of the target (new) mesh element is determined based on a weighted average of the values of the donor (old) mesh. The weight function reflects the fraction of the Gauss volume of each donor element located inside the target Gauss volume (Gauss point in evaluation). However, this strategy carries the difficult problem of calculating intersecting elements volumes belonging to distinct meshes (see Fig. 2) [15,32]. This issue is surpassed by using an incremental volumetric scheme [19] to determine the intersecting volume between two finite elements.

The procedure starts with the division of both finite element meshes in Gauss volumes as shown in Fig. 1(a) and (b). Subsequently, the Gauss volumes of the target mesh are divided into a predefined number of parts (Fig. 1(c)), defined by the *nl* parameter. The centroid of each small part of the target Gauss volume is evaluated resorting to the parametric inversion of the shape functions. The volume coordinates method is applied to define which donor Gauss volume contains this centroid (Fig. 2(c)). This straightforward method avoids higher time consuming iterative algorithms, such as the ones based on the parametric inversion of the element shape functions [19]. The state variable assigned to each single target Gauss volume part is equal to the one of the donor Gauss volume, in which the volume part centroid is located, as shown in Fig. 2(c). The number of donor Gauss volumes that contributes for the target Gauss volume (in evaluation) is given by the parameter *ng*, which, for the case presented in Fig. 2(c), is equal to two. The value α of the state variable in a Gauss point of the target element is given by:

$$\alpha = \sum_{i=1}^{ng} \frac{\sum_{j=1}^{nl^3} V_{j,i}}{V_{tot,j}} \alpha_i, \tag{1}$$

where $V_{j,i}$ is the j Gauss volume part of the target mesh contained in the donor Gauss volume i; $V_{tot,j}$ is the total volume of the target Gauss volume j and α_i is the state variable quantity of the i donor Gauss volume. Note that, since each target Gauss Volume is subdivided into *nl* equal subdivisions in each direction, it yields a total of nl^3 divisions per element (Fig. 1(c)). In brief, the volumetric weighting of the variables in the new mesh (Fig. 2(c)) is given by the intersection between the donor Gauss volumes and the centroid of each sub-volume. Previous results indicate that the increase of the *nl* parameter, which allows the control of the remapping accuracy, increases the computational time exponentially, while the error reduction stabilizes for values greater than five [18,30]. Thus, this value is assumed for the *nl* parameter in this work. Moreover, this method only enables the proper remapping of scalar quantities, i.e. if the state variable is a tensor each component is remapped independently. This may cause inaccuracies in the remapping of tensor variables.

2.2. Dual Kriging (DK) method

Kriging is a geostatistical method developed by Krige [33] and Matheron [34]. This method and consequently the ones based on it, presents two main characteristics: it is the best linear unbiased estimator of a variable and also an exact interpolator. The exact interpolator property ensures that, when the original coordinates are provided, the interpolation method will return the original values (self-consistency). In fact, this is the main advantage of this method over the moving least square interpolation. The Dual Kriging version is applied in the present study as it provides an explicit parametric interpolation formula to compute the interpolation value α for any point with Cartesian coordinates $\mathbf{x}_t = [x \quad y \quad z]^T$ [31,35,36]. In the context of this work, this point denotes the target Gauss point (GP). The interpolation function can be decomposed in two terms:

$$\alpha(\mathbf{x}_t) = d(\mathbf{x}_t) + f(\mathbf{x}_t). \tag{2}$$

The first term is named the drift, $d(\mathbf{x}_t)$, and it represents the average or global trend of $\alpha(\mathbf{x}_t)$. It is usually a linear polynomial function, obtained from a scalar product such as:

$$d(\mathbf{x}_t) = \mathbf{d} \cdot \begin{bmatrix} 1 \\ \mathbf{x}_t \end{bmatrix} = d_1 + d_2 x + d_3 y + d_4 z, \tag{3}$$

where $\mathbf{d}$ is the vector composed by the coefficients that define the average plane derived from the known values at the seed points, i.e. donor GPs. Thus, the linear drift is correlated to this plane. In 2D applications, the last term of $\mathbf{x}_t$, z, and of $\mathbf{d}$, d_4, are removed. The second part of Equation (2) represents the fluctuation or deviation, $f(\mathbf{x}_t)$, from $d(\mathbf{x}_t)$, associated with each seed point:

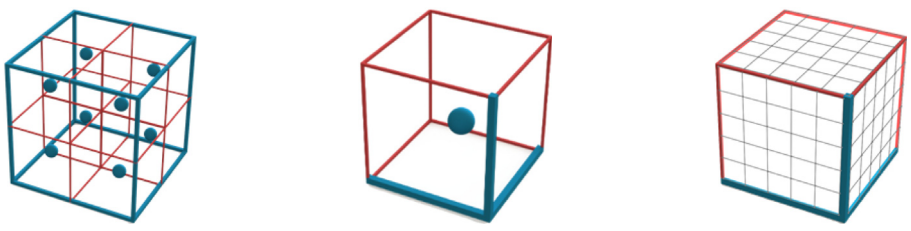

Fig. 1. Subdivision of the finite element mesh. (a) element partition in Gauss Volumes (GPs in blue circles); (b) single Gauss Volume; (c) partition of the target Gauss Volume in *nl* equal subdivisions in each direction (Adapted from Ref. [30]). (For interpretation of the references to colour in this figure legend, the reader is referred to the web version of this article.)

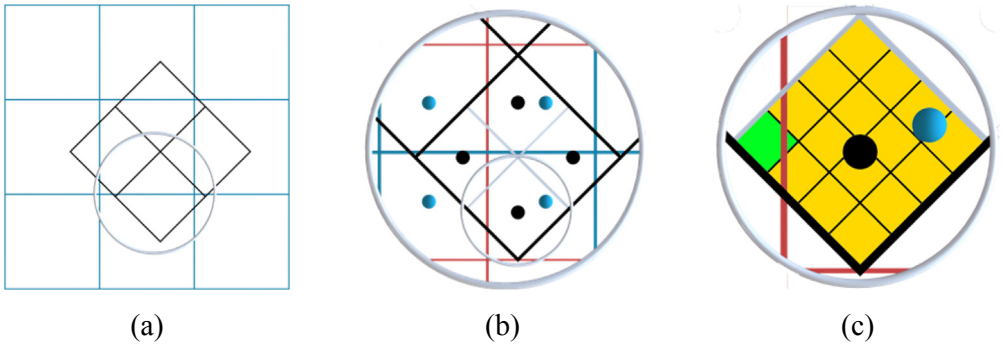

Fig. 2. 2D schematic of the IVR method with donor (blue) and target (black) meshes: (a) detail of one target element; (b) partition of the donor and target elements into Gauss Volumes and detail of one target Gauss Volume; (c) partition of the target Gauss Volume in nl^3 sub-volumes and evaluation of each donor Gauss Volume (Adapted from Ref. [30]). (For interpretation of the references to colour in this figure legend, the reader is referred to the web version of this article.)

$$f(\mathbf{x}_t) = \sum_{i=1}^{n} \lambda_i K(h_{ti}) = \sum_{i=1}^{n} \lambda_i K(|\mathbf{x}_t - \mathbf{x}_{d_i}|), \tag{4}$$

where n is the total number of seed points, $\mathbf{x}_{d_i}$, i.e. donor GPs; K is the generalized covariance function, which can assume different forms, but it is always a function of the Euclidean norm (h_{ti}) between the target GP (t) and each donor GP (d_i); and λ is a weighting factor associated with each donor GP. Thus, the general form is obtained by replacing Equations (3) and (4) into Equation (2):

$$\alpha(\mathbf{x}_t) = d_1 + d_2 x + d_3 y + d_4 z + \sum_{i=1}^{n} \lambda_i K(|\mathbf{x}_t - \mathbf{x}_{d_i}|). \tag{5}$$

To define this function, it is necessary to solve a system $n+s+1$ of linear equations, where s defines the space dimension, two for 2D problems and three for 3D. This system is given by:

$$\mathbf{K}\mathbf{u} = \mathbf{f} \Leftrightarrow \mathbf{u} = \mathbf{K}^{-1}\mathbf{f}, \tag{6}$$

where $\mathbf{K}$ is called the Kriging matrix, $\mathbf{u}$ is the vector of unknowns, and $\mathbf{f}$ contains the values of the variable in the seed points (for further details see e.g. Refs. [31,35,36]). The vector of unknowns is composed by n weighting factors λ_i and the $s+1$ scalar quantities that define the vector $\mathbf{d}$. The symmetric square dense matrix $\mathbf{K}$, with null diagonal, can be divided into four submatrices, each with a different dimension:

$$\begin{bmatrix} \mathbf{K}_{11} & \mathbf{K}_{12} \\ \mathbf{K}_{21} & \mathbf{K}_{22} \end{bmatrix} \times \mathbf{u} = \mathbf{f} \Leftrightarrow \begin{bmatrix} K(|\mathbf{x}_{d_i} - \mathbf{x}_{d_j}|) & \begin{matrix} 1 & \mathbf{x}_{d_1}^T \\ \vdots & \vdots \\ 1 & \mathbf{x}_{d_n}^T \end{matrix} \\ \begin{matrix} 1 & \cdots & 1 \\ \mathbf{x}_{d_1} & \cdots & \mathbf{x}_{d_n} \end{matrix} & \begin{matrix} 0 & \cdots & 0 \\ \vdots & \ddots & \vdots \\ 0 & \cdots & 0 \end{matrix} \end{bmatrix} \times \begin{bmatrix} \lambda_1 \\ \vdots \\ \lambda_n \\ d_1 \\ \vdots \\ d_s \end{bmatrix} = \begin{bmatrix} f_1 \\ \vdots \\ f_n \\ 0 \\ \vdots \\ 0 \end{bmatrix}, \tag{7}$$

where $\mathbf{K}_{11}$ is the biggest submatrix, with dimension $n \times n$, containing the covariance values between each donor point, i.e. $\mathbf{K}_{11} = K(h_{ij})$, $i,j = 1,\ldots,n$. As previously mentioned, these values depend on the covariance function selected. $\mathbf{K}_{21} = \mathbf{K}_{12}^T$, is a matrix with dimension $(s+1) \times n$, with the first row equal to one and the coordinates x, y and z of each donor GP in the second, third and fourth column, respectively. The number of rows of this matrix depends on the space dimension $s+1$. $\mathbf{K}_{22}$ is a square matrix with the same dimension as the number of rows of $\mathbf{K}_{21}$, $(s+1) \times (s+1)$, and always contains only null values.

The accuracy of the results provided by the Dual Kriging method is significantly affected by the covariance function selected, as shown by McLean et al. [31]. They compared three different functions and concluded that the most consistent results were given by the Euclidean distance, which is also adopted in the present work:

$$K(h) = h = |\mathbf{x}_t - \mathbf{x}_{d_j}|. \tag{8}$$

The (Dual) Kriging is a global interpolation method, i.e. the interpolation function can be evaluated only once for the whole domain using the information of all donor points [31,36,37]. Nevertheless, this procedure is not mandatory, which can help save some computational time, since the inversion of very large matrices is time-consuming. Furthermore, whatever the number of donor points selected, as long as this set remains unchanged, once the Kriging matrix is inverted (see Equation (6)), it is only necessary to update the values of the variable to be remapped from the donor GP points (vector $\mathbf{f}$) in order to obtain the coefficients required to evaluate its value for the target GP (using Equation (5)). Thus, unlike the strategy adopted in the IVR method, where the same weight value is applied in the remapping of all state variables, Kriging interpolation evaluates the drift and the fluctuation associated with each state variable (see Equation (2)).

The computational performance of the Dual Kriging method depends on the size of the linear system of equations to be solved, which in turn depends on the number of donor GPs (n) selected to interpolate each target GP. Direct inversion can be applied for small rank matrixes, but bigger require a direct or an iterative solver, due to the non-linear scaling of the required computational time of the direct inversion. In this work, the system of linear equations (see Equation (6)) is solved through the matrix inversion, since this enables a faster evaluation of the Kriging interpolation parameters for several state variables, as long as the set of donor GPs remains unchanged, as previously mentioned. Although the Kriging matrix is not positive definite (see Equation (7)), the inversion performed with a direct method using subroutines from LAPACK library [38] was performed without issues.

The implementation of Kriging as a remapping method, applied to each target GP, can be divided into three stages: (i) selection of a set of neighbour donor GPs; (ii) evaluation of the Kriging coefficients and weighting factors; and (iii) evaluation of each state variable value in the target GP. In the first stage, similarly to many numerical methods that allow for a flexible amount of inputs, the problem of overfitting or underfitting is present. Generally, overfitting can occur when a mathematical function is forced to intercept too many points, while underfitting occurs when there are not enough points to provide a good representation of the domain. It is also important to consider the discontinuous nature of the variables, since continuity is ensured inside the element but not outside. These two factors oppose the use of a brute force method, i.e. simultaneous use of all donor mesh's GPs. Thus, the alternative is to search for a limited number of donor GPs in the neighbourhood. Besides improving accuracy, this also reduces the

computational cost of the method, by limiting the number of seed points.

Several selection algorithms for choosing the set of donor GPs were tested, the most promising being referred as Master-Slave and Planar methods, which will be described in the following sections (for further details on other selection methods please refer to Diogo [39]). Both involve the knowledge of the mesh connectivity and the evaluation of the Cartesian coordinates of the donor and target GPs, which in turn enable the subsequent assembly of the Kriging matrix **K**, its inversion in the second stage of the remapping method, and use of the calculated values to evaluate the state variable(s) for the target GP. The global algorithm of the Dual Kriging remapping method, as well as the foremost nomenclature used by both selection methods is defined in Table 1. Both methods try to avoid underfitting, overfitting and discontinuity problems, while keeping their simplicity and efficiency, by considering the connectivity of the donor finite element mesh. These procedures are based on the relative position of the target GP in the donor mesh. Thus, the nearest node of the donor mesh to the target GP is determined to define the Master Node. The selection of the Master node allows the definition of the donor finite element, based on the donor mesh connectivity and the parametric inversion of the shape functions. The donor finite element that contains the target GP is defined as the Master Element and all other elements that share the Master Node are defined as Slave Elements. The two proposed methods differ in the way the donor GPs are selected from the set of GPs belonging to the Master and Slave Elements, denoted by Master and Slave GPs, respectively (see Table 1).

2.2.1. Master-Slave selection method

In this selection method, the set of donor GPs includes all the GPs of the Master Element. For each Slave element, the set of donor GPs is defined based on its relative position to the Master Element, i.e. the number of donor GPs is different for a Slave Element that shares a facet, an edge or a vertex with the Master Element. The selection of the GPs is performed based on the fact that there is a direct correspondence between the FE connectivity and the GPs numbering. The idea is to select a reduced number of GPs while ensuring the creation of an envelope, i.e. the GPs of the finite element containing the target GP and particular GPs of some neighbouring finite elements. Moreover, the methodology was developed to use, at most, three GPs in each orthogonal direction of the finite element, allowing a non-linear interpolation. Thus, this approach tries to minimize problems of overfitting and underfitting. Table 2 presents the outline of the Master-Slave selection method and Fig. 3(a) shows an example of the selection of the GPs from the Slave Elements. In this figure, the target GP is located inside the Master Element that corresponds to the left inferior posterior quadrant (omitted to simplify the visualization). The Master Node, shared by the Slave Elements is represented in black. The set of donor GPs (see Fig. 3(a)) is composed by: (i) eight GPs of the Master Element (omitted); (ii) four GPs of each Slave Element with only one shared facet (in blue); (iii) two GPs of each Slave Element with only one shared edge (in green); and (iv) one GP of each Slave Element with only one shared vertex (in red). For this example, the set of donor GPs is composed by eight GPs from the Master Element and nineteen from the Slave Elements, i.e. presents a total of 27 donor GPs ($n = 27$). When using this selection method, this corresponds to the maximum number of donor GPs allowed. Therefore, in this work, the Kriging matrix is inverted directly due to its small overall size.

Table 1
Outline of the algorithm adopted in the Dual Kriging remapping methods, highlighting the structure corresponding to the selection of the set of neighbouring donor GPs.

For each target GP $\mathbf{x}_t$:	
Selection Stage	1. Determine the closest node from the donor mesh (**Master Node**), based on the Euclidean distance;
	2. Determine the set of finite elements from the donor mesh that share the Master Node, based on the FE connectivity; 2.1. Define the donor mesh FE that contains the target GP (**Master Element**), based on the canonical coordinates of the target GP; 2.1.1. Define the set of donor mesh's GPs belonging to the Master Element (**Master GPs**); 2.2. Define the donor mesh FE that share the Master Node, but do not contain the target GP (**Slave Elements**), based on the canonical coordinates of the target GP; 2.2.1. Define the set of donor mesh's GPs that belong to any Slave Element (**Slave GPs**);
	3. Build the Kriging matrix **K** (see Equation (7)) and calculate its inverse. 4. For each state variable: 4.1. Build the second member vector, **f** (see Equation (7)); 4.2. Determine the weighting factors λ_i and the vector **d** (see Equation (6)); 4.3. Determine the value of the state variable for the target GP $\alpha(\mathbf{x}_t)$ (see Equation (5)).

Table 2
Outline of the Master-Slave selection method.

For each FE associated with the target GP $\mathbf{x}_t$ (see Table 1):
If FE = Master Element **Then**
  Add to the set of donor GPs the eight GPs of the Master Element
Else If FE=Slave Element **Then**
  IF the Slave element shares a facet with the Master Element **Then**
    Add to the set of donor GPs the four GPs corresponding to the shared facet
  IF the Slave element shares an edge with the Master Element **Then**
    Add to the set of donor GPs the two GPs corresponding to the shared edge
  IF the Slave element shares a vertex with the Master Element **Then**
    Add to the set of donor GPs the GP corresponding to the shared vertex
End If

2.2.2. Planar selection method

This selection method may be considered as a particular case of the Master-Slave since it considers the same group of Slave Elements, but only the GPs located in the same layer of the target GP are taken into account. Thus, although similar to Master-Slave, it does not consider the influence of GPs located in layers different from the target GP. Its implementation considers the geometry of the brick element and the assumption that the FE mesh corresponds to a thin sheet metallic blank, typically used in the simulation of the deep-drawing processes. Thus, it is possible to determine in which direction the finite elements were stacked to define the blank thickness, based on the geometrical information of the brick FE mesh, internally generated and stored in the form of connectivity tables for its facets [40]. Moreover, it is possible to identify the edges that are aligned with the stacking (thickness) direction. This allows the determination of the Reference Facet of the Master Element, i.e. the facet defined by the two edges that contain the Master Node that are not aligned with the thickness direction. The other edge of the Master Element defined with the Master Node will be labelled Reference Edge since it is the one aligned with the thickness direction.

In this selection method, the set of donor GPs includes only four GPs of the Master Element, which are associated with the nodes that define the Reference Facet for the target GP. For each Slave element, the set of donor GPs is defined based on its relative position to the Master Element, i.e. the number of donor GPs is different for a Slave Element that shares a facet or an edge. Table 3 presents the outline of the Planar selection method and Fig. 3(b) shows an example of the GPs selection. In this case, the target GP is located inside the Master Element, presented in blue. The Master Node, shared by the Slave Elements is represented in black. The set of selected donor GPs is composed by: (i) four GPs of the Master Element located in the Reference Facet (in blue); (ii) two GPs of each Slave Element that shares the Reference Edge and one edge of the Reference facet (in green); and (iii) one GP of each Slave Element that shares only the Reference Edge (in red). Thus, for the same target GP used in Fig. 3(a), the planar method leads to nine donor GPs, i.e. presents a total of 9 donor GPs ($n = 9$), as shown in Fig. 3(b). Although this selection method was developed with a specific application in mind, it can be applied to any remapping problem that involves donor and target meshes that present the same discretization in one particular direction. In such case, that direction is assigned as the thickness one.

Two implementations were tested for the planar selection remapping

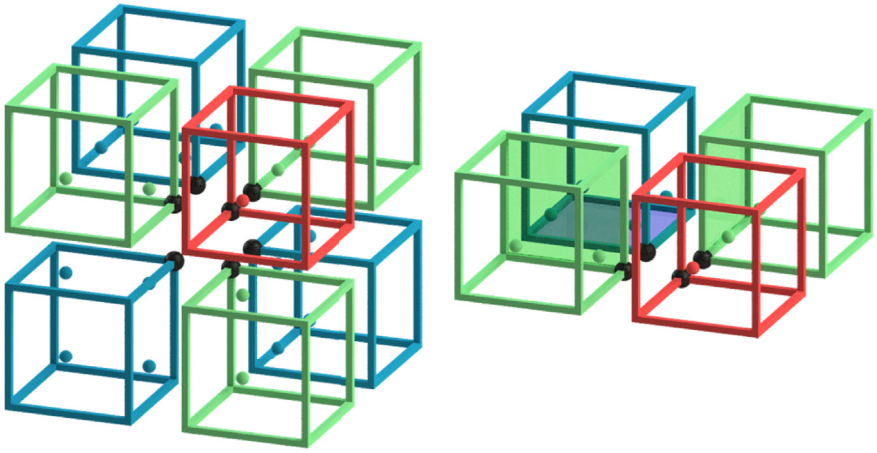

Fig. 3. Comparison of donor GPs' sets for both Kriging methods, for a target GP located in the left bottom quadrant. The Master Node, shared by the Slave Elements, is represented in black: (a) Master-Slave method (Master Element and its eight GPs are omitted); (b) Planar selection method.

Table 3
Outline of the Planar selection method.

For each FE associated with the target GP $\mathbf{x}_t$ (see Table 1):
If FE = Master Element **Then**
  Add to the set of donor GPs the four GPs of the Master Element, corresponding to the Reference Facet
Else If FE=Slave Element **Then**
  IF the Slave element shares the Reference Edge and an edge of the Reference Facet with the Master Element **Then**
    Add to the set of donor GPs the two GPs corresponding to the shared edge of the Reference Facet
  IF the Slave element shares only the Reference Edge with the Master Element **Then**
    Add to the set of donor GPs the GP corresponding to the Master Node
End If

method, the difference being the spatial domain: $\Re^3$ and $\Re^2$. In the first approach the 3D Cartesian coordinates of each GP were supplied directly, i.e. the dimension of the $\mathbf{K}_{21} = \mathbf{K}_{12}^{\mathrm{T}}$ matrix was $n \times (3+1)$. However, since the foundation of this method is that the reference plane is the same, the 3D coordinates can be converted to a plane and then converted to a 2D coordinate system, leading to a matrix of dimension equal to $n \times (2+1)$. To evaluate this reference plane, two vectors are created based on the Master GP (corresponding to the Master Node) and the two GPs belonging to the adjacent edges in the Reference Facet. The cross product of these two vectors defines the normal vector, perpendicular to the Reference Facet, which in turn contains the initial vectors. To correct offsets from this reference plane to GPs of the adjacent elements, due to bending, two correction methods were evaluated: the projection of the converted coordinates along the normal vector and the rotation about the nearest initial vector. Both strategies lead to similar results and, consequently, the results presented in this work correspond to the adoption of the projection to the 2D plane.

Regarding the two spatial domain implementations ($\Re^3$ and $\Re^2$), for the tested examples, it was found that the conversion to a 2D coordinate system provides more accurate results. In fact, the adoption of a 3D coordinate system can introduce some spurious gradients, due to the poor conditioning of the matrix, as there will be two linearly dependent rows (and columns): the row of ones and the row that defines the constant coordinate (see Equation (7)).

3. Remapping examples

This section presents the comparison of both approaches of the Dual Kriging remapping method with the IVR method, both in terms of accuracy and computational cost. The first example analysed deals with the remapping between two different finite element meshes. The geometry studied is a disk with 100 mm of radius and 1 mm of thickness. It is discretized with hexahedral elements (eight nodes and eight GPs), using both structured and unstructured in-plane meshes, shown in Fig. 4(a) and (b) respectively. The remapping is carried out in two stages. First, from the structured to the unstructured mesh (called stage 1) and afterwards, back to the structured mesh (called stage 2). In order to quantify the error associated with the remapping method, each GP of the meshes was initially mapped with the following scalar analytical function [10,11,15]:

$$T(r,\theta) = 20r^2(r-1)^2\cos(2\theta); \quad r = \sqrt{\frac{x^2+y^2}{a^2}}, \tag{9}$$

where r and θ are the polar coordinates, x and y the Cartesian coordinates of each GP, and a is the radius of the disk. Based on this definition, the relative error associated with the remapping method E is defined as:

$$E(r,\theta) = \frac{T(r,\theta) - \alpha(\mathbf{x}_t)}{\max(T(r,\theta))} = \frac{T(r,\theta) - \alpha(\mathbf{x}_t)}{1.25}, \tag{10}$$

where T is the value given by the analytical function (9) and α is the interpolated value provided by the remapping method. The classical definition of relative error is not adopted in the present analysis because the analytical function (9) is null at some points. First, the analytical distribution (9) is considered uniform through the thickness. After that, a gradient along the thickness is considered in the second case, i.e. the local value of T is multiplied by a coefficient depending on the position of the GP along the thickness direction. Since both finite element meshes contain two layers of elements through the thickness (four GPs along this direction), the distribution is: T, $0,1 \times T$, $-0,1 \times T$, and $-T$, from the top to the bottom layer. Fig. 4 presents the distribution of the analytical function adopted in the present study, highlighting the difference in terms of mesh density. Since the size of the finite elements in-plane is significantly different between the two meshes, the remapping operation can be interpreted as a mesh refinement of the discretization.

3.1. Accuracy

Considering the case without gradient along the thickness, Fig. 5 presents the relative error distribution on the disk, comparing the three remapping methods. The contour plots are obtained with the GiD post-processor [41] using the input values given in the GPs, which are

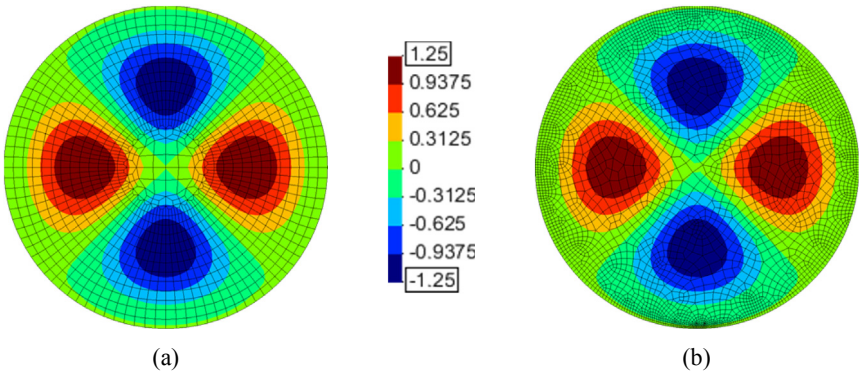

Fig. 4. Distribution of the scalar variable on both finite element meshes (2 layers of elements through the thickness): (a) mesh 1 composed by 2688 elements (21,504 GPs) and 4179 nodes; (b) mesh 2 composed by 6694 elements (53,552 GPs) and 10,575 nodes.

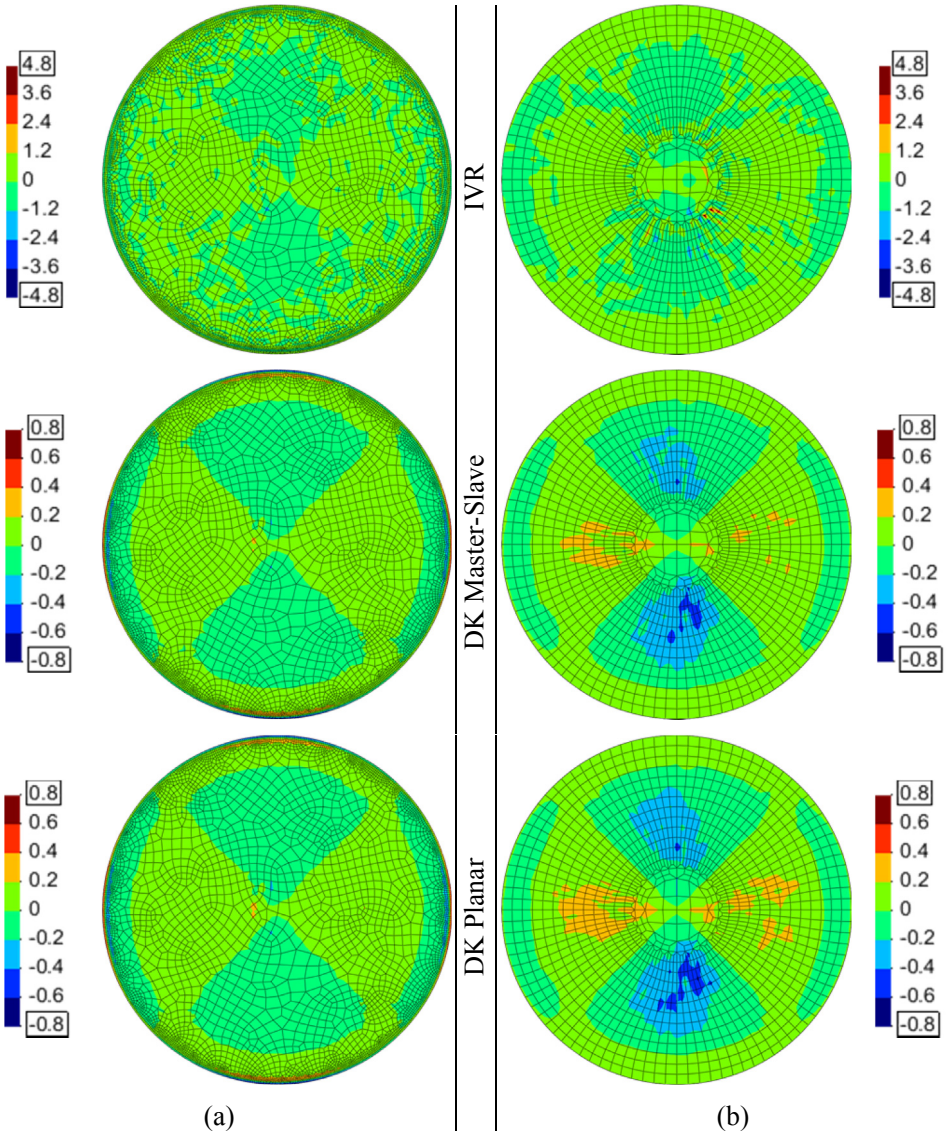

Fig. 5. Distributions of relative error in each remapping operation: (a) stage 1; (b) stage 2, comparing the Incremental Volumetric Remapping (IVR), Dual Kriging Master-Slave and Planar Dual Kriging. No function gradient through the thickness.

smoothed to the mesh surface. Concerning the first remapping operation (stage 1), both Dual Kriging remapping methods (Master-Slave and Planar) provide similar error distribution, as shown in Fig. 5 (a). The large values of error are located close to the outer boundary, because of the extrapolation resulting from the difference in the in-plane element size between the original and the target mesh. On the other hand, the IVR

method is less sensitive to the change of the in-plane mesh size, presenting a uniform error distribution in the outer boundary (see Fig. 5(a)). Indeed, the maximum error values are located near the zone where the donor mesh presents the change in topology. Regarding the second remapping operation (stage 2), both Dual Kriging remapping strategies provide similar results, as shown in Fig. 5(b). Since the in-plane element size of the target mesh is larger than the one of the donor mesh, no extrapolation occurs in the outer boundary zones. Furthermore, the comparison between Master-Slave and Planar methods allows the observation of a slight improvement when the Master-Slave method is applied, because it uses several GPs along the thickness (z) with identical values. The IVR method presents slightly bigger error values, namely in the areas where the target mesh presents smaller in-plane elements and near the zone corresponding to the transition between mesh topologies.

The histogram of error is shown in Fig. 6 for each stage, comparing the three remapping methods under analysis. The maximum values of relative error, evaluated in the GPs, are contained in Table 4. Considering the stage 1 (Fig. 6(a)), both forms of Dual Kriging interpolation provide identical error distribution for both stages. Moreover, they provide a smaller error dispersion in comparison with the IVR method, both in terms of maximum (positive) and minimum (negative) error values. Regarding the error distribution in stage 2, it is possible to conclude that the IVR method exhibits the higher error values, such as observed in stage 1 (see Fig. 6). On the other hand, the range of the remapping error is similar for the Master-Slave and Planar methods. Nevertheless, the remapping error range exhibited by the IVR method is significantly larger in stage 2 than in stage 1, as shown in Fig. 6.

Regarding stage 1, both the Master-Slave and the Planar methods present 88% and 98% of the GPs with relative error inferior to 0.25% and to 0.5%, respectively. On the other hand, about 50% of the GPs present a relative error smaller than 0.25% when adopting the IVR method, while 20% of them presents error values between 0.25% and 0.5%. Regarding stage 2, both the Master-Slave and the Planar methods provide 99% of the GPs with a relative error smaller than 0.5%. For the IVR method, around 60% of GPs present an error inferior to 0.5%. This highlights the ability of these remapping methods to transfer variables accurately from coarse to fine meshes (stage 1) and *vice-versa* (stage 2).

Considering the gradient of the analytical function through the thickness, Fig. 7 presents the error distributions obtained by each remapping method for the two stages. For stage 1, the distribution obtained with the Master-Slave method presents the highest spread and error value, while the Planar method presents the lowest. In fact, the

Table 4
Maximum relative error values for the case without through-thickness gradient.

Stage 1		Relative Error	Stage 2		Relative Error
IVR	Max	4.25%	IVR	Max	8.63%
	Min	−4.97%		Min	−8.08%
Master-Slave	Max	0.68%	Master-Slave	Max	0.67%
	Min	−0.75%		Min	−0.83%
Planar	Max	0.68%	Planar	Max	0.68%
	Min	−0.76%		Min	−0.86%

Planar and the IVR remapping methods present error distributions similar to the one obtained for the case without a through-thickness gradient (see Fig. 5 (a)).

Regarding stage 2, the IVR method presents an error distribution identical to the one obtained in stage 1 (see Fig. 7). The Planar selection method shows an increase in the error dispersion in comparison with stage 1. From the error frequency analysis (see Fig. 8), it is possible to conclude that the Master-Slave method presents the highest overall error and spread in both stages, while the Planar selection method has the lowest. When comparing with stage 1, the extreme values of the error (see Table 5) increase for both the IVR and the Planar selection method, although slightly for the latter. For the Master-Slave the error range decreases. Considering the application of the Planar selection method, all GPs present a relative error inferior to 0.9% in both stages (see Table 5), 99% of which with an error below 0.5%. On the other hand, 93% of GPs present an error lower than 0.9% by applying the IVR method in stage 1, 85% below the 0.5% threshold, which reduces to about 81% and 68%, respectively, when the Master-Slave method is applied. In stage 2, these ratios decreased to about 89% and 79% for IVR, and approximately 48% and 36% for Master-Slave, respectively for 0.9% and 0.5%. The maximum values of relative error (see Table 5) increased slightly for Planar, and more significantly for IVR while decreasing for Master-Slave. Nevertheless, the Master-Slave method provided the highest error values and worst global results, when considering the gradient of the analytical function through the thickness.

Comparing the results obtained for both cases (without and with through-thickness gradient) it can be concluded that the error distribution obtained with the Planar selection method is only slightly affected by the gradient through the thickness. The IVR method presents larger zones with significant error values. As for the Master-Slave selection method, the error distribution is strongly affected by the gradient, resulting in a wider spread and higher values. In fact, adding the

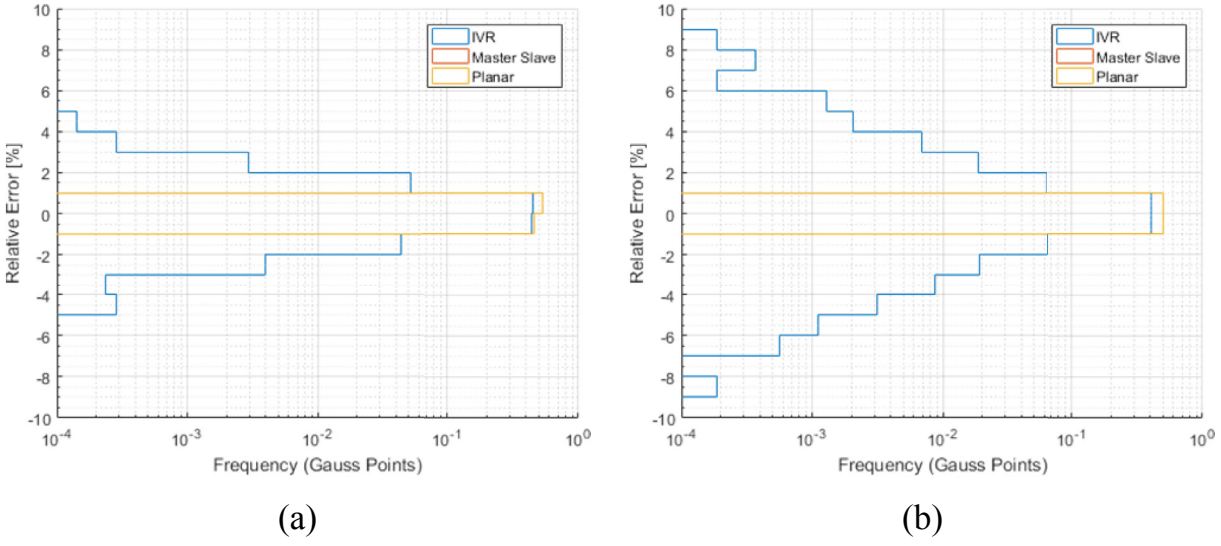

Fig. 6. Histograms of the relative error in the remapping for the case without through-thickness gradient: (a) stage 1; (b) stage 2. The frequency is normalised with the total number of target GPs.

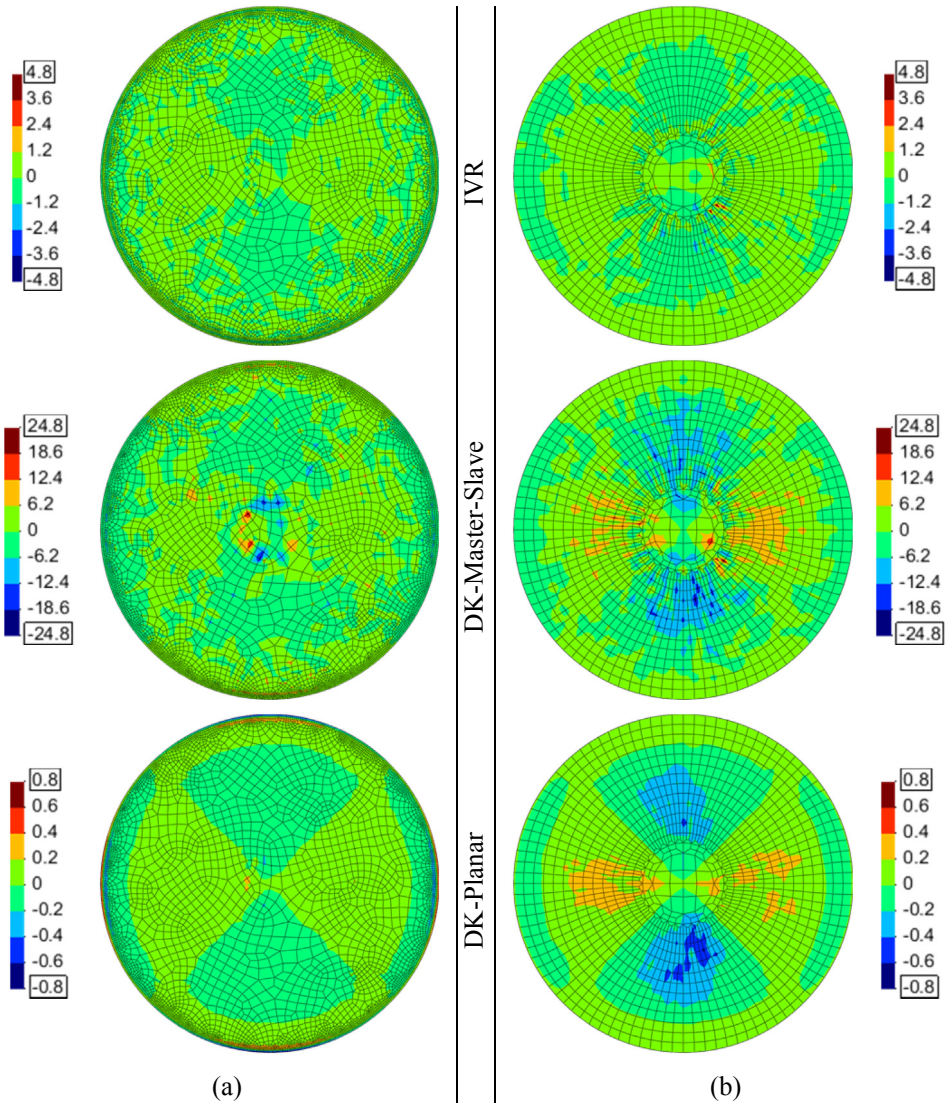

Fig. 7. Distributions of relative error in each remapping operation: (a) stage 1; (b) stage 2, comparing the Incremental Volumetric Remapping (IVR), Dual Kriging Master-Slave and Planar Dual Kriging. Function gradient through the thickness.

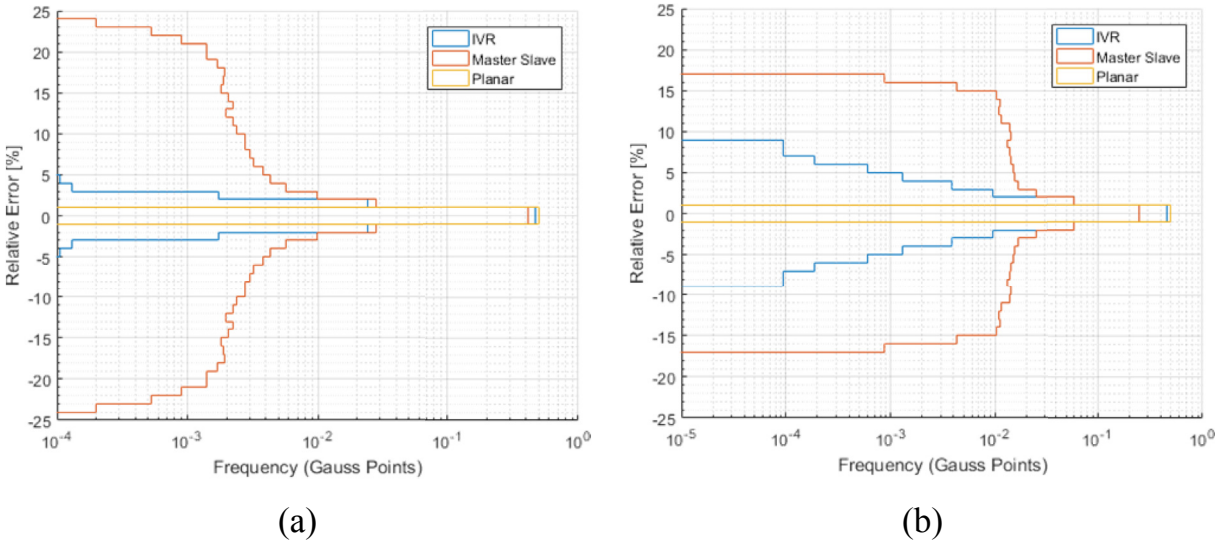

Fig. 8. Histograms of the relative error in the remapping for the case with through-thickness gradient: (a) stage 1; (b) stage 2. The frequency is normalised with the total number of target GPs.

Table 5
Maximum relative error values for the case with a through-thickness gradient.

Stage 1		Relative Error	Stage 2		Relative Error
IVR	Max	4.97%	IVR	Max	8.63%
	Min	−4.97%		Min	−8.63%
Master-Slave	Max	23.71%	Master-Slave	Max	16.62%
	Min	−23.71%		Min	−16.62%
Planar	Max	0.76%	Planar	Max	0.86%
	Min	−0.76%		Min	−0.86%

thickness gradient, the error distribution frequency and extreme values increased for all methods. However, while the IVR and the Planar selection methods present errors with similar orders of magnitude, the Master-Slave method showed poorer performance in the through-thickness gradient case. This arises from the relative dimensions of the mesh, i.e. the size of the elements is much bigger in the in-plane directions than along the thickness, which leads to an overweighting of the through-thickness direction component. It should be mentioned that, when applying the Master-Slave method in the example with the gradient along the thickness direction, the extreme error values occur in the interior GPs. However, as shown in Fig. 7, the GPs located on the surface also present significant error values when compared to the example without the gradient (see Figs. 5 and 7). Additionally, the maximum relative errors obtained with Planar and Master-Slave methods in stage 2 are in the same locations. Comparing both meshes it is clear that the dominating factor for the accuracy is the relative dimension of the finite elements.

In order to assess the influence of the mesh refinement on the remapping accuracy, two distinct meshes were generated, a coarse mesh composed by 2472 finite elements (see Fig. 9(a)) and a fine mesh composed by 27,072 finite elements (see Fig. 9(b)). The self-consistency condition of all remapping methods was confirmed by mapping from a mesh onto itself (for both meshes), which lead to relative errors lower than 10^{-10}. The relative error distribution arising in the remapping from the fine to the coarse mesh is presented in Fig. 9(a), comparing the IVR and the Dual Kriging Master-Slave. While the relative error distribution in the remapping from the coarse to the fine mesh is presented in Fig. 9(b), using the same remapping methods. For both remapping methods, the error is substantially higher when the donor mesh is coarser than the target one, as highlighted in Fig. 10. Nevertheless, the accuracy of the Master-Slave method is about an order of magnitude higher than the one obtained with the IVR. The maximum values of relative error, evaluated in the GPs, are presented in Table 6, comparing both Dual Kriging remapping methods (Master-Slave and Planar) and the IVR. Both the Master-Slave and Planar selection methods present identical levels of accuracy since the function presents no through-thickness gradient.

3.2. Computational performance

The computational cost associated exclusively with the remapping operation was evaluated and is presented in Table 7, for both examples. For the implemented Dual Kriging methods, it is important to mention that: (i) the Master-Slave method selects a higher number of donor GPs; thus, (ii) the maximum dimension of the Kriging matrix differs, i.e. for the Planar selection method is 12 × 12, while for the Master-Slave is 31 × 31; nonetheless, (iii) the Planar selection method requires the conversion from 3D to a 2D (planar) coordinate system.

Both Dual Kriging remapping methods are significantly faster than the IVR method, as shown in Table 7. At least 87% of the computational time can be saved for non-matching meshes, i.e. meshes that have no relation between them and, therefore, require an intersection algorithm to identify the relationship between donor and target elements. Nevertheless, it should be noted that all implementations adopted in these methods are serial, which means that it is possible to improve their computational time. The existence (or absence) of the through-thickness gradient has no effect on the computational time because the number of operations involved is the same in both cases.

The difference in computational time between *stage 1* and *stage 2* is

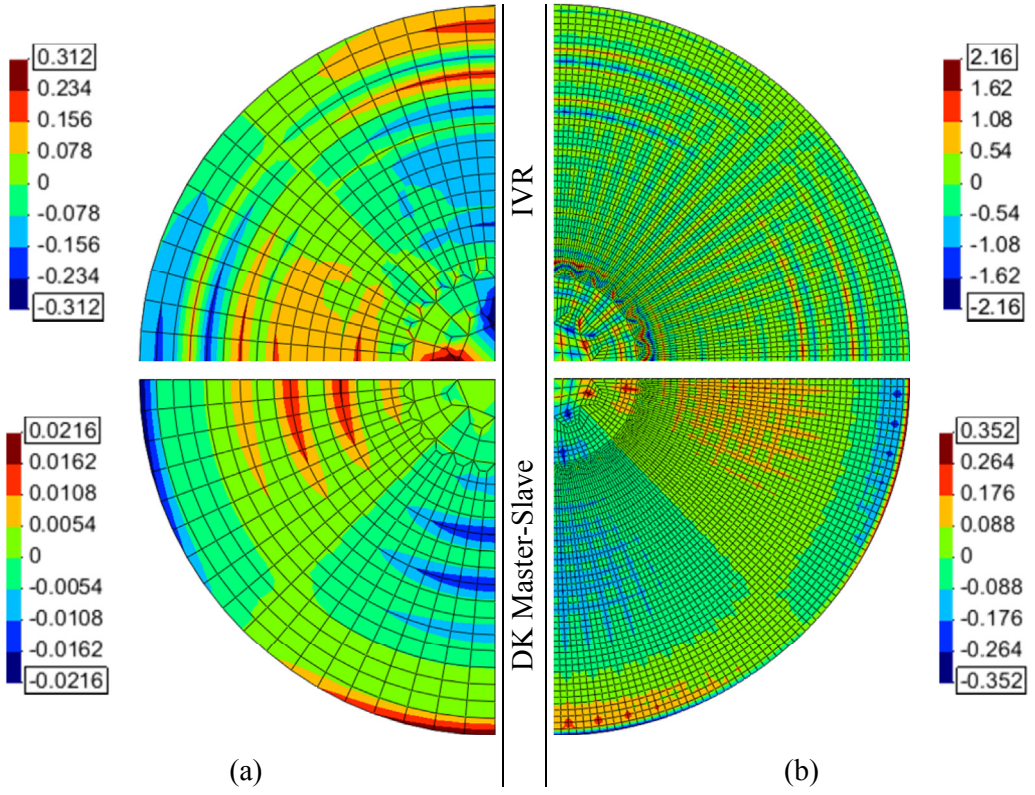

Fig. 9. Distributions of relative error in each remapping operation: (a) from fine to coarse; (b) from coarse to fine, comparing the Incremental Volumetric Remapping (IVR) and Dual Kriging Master-Slave. No function gradient through the thickness.

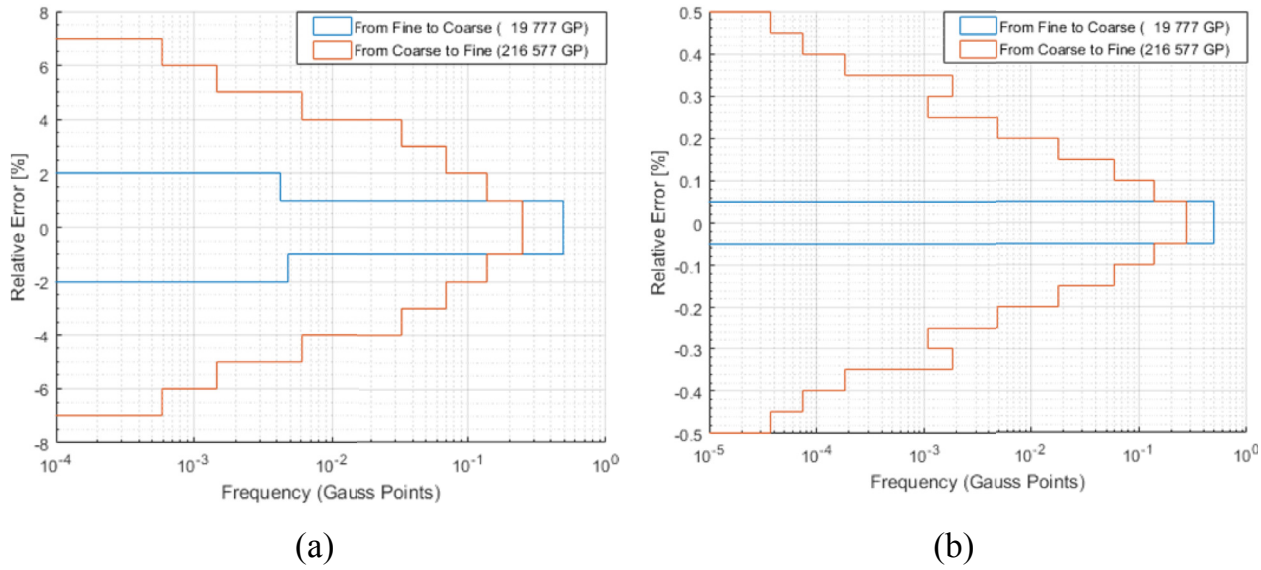

Fig. 10. Histograms of the relative error in the remapping involving distinct meshes and analytical function without through-thickness gradient: (a) Incremental Volumetric Remapping (IVR); (b) Dual Kriging Master-Slave. The frequency is normalised with the total number of target GPs.

Table 6
Maximum relative error values for the case comprising distinct meshes and analytical function without through-thickness gradient.

From fine to coarse		Relative Error	From coarse to fine		Relative Error
IVR	Max	1.180%	IVR	Max	6.930%
	Min	−1.180%		Min	−6.930%
Master-Slave	Max	0.021%	Master-Slave	Max	0.464%
	Min	−0.021%		Min	−0.464%
Planar	Max	0.026%	Planar	Max	0.496%
	Min	−0.026%		Min	−0.496%

Table 7
Computational time (in seconds) and relative difference of the Dual Kriging methods to IVR in brackets.

	Without Gradient		With Gradient	
	Stage 1	Stage 2	Stage 1	Stage 2
IVR ($nl = 5$)	216	197	216	197
Master-Slave	29 (13%)	24 (12%)	29 (13%)	24 (12%)
Planar	23 (11%)	22 (11%)	23 (11%)	22 (11%)
Number of GPs	53,552	21,504	53,552	21,504

Average time for 12 executions on an i7-4860HQ 2.40–3.20 GHz, always discarding two extreme values. Values rounded.

dictated by the number of GPs that need to be evaluated and the donor mesh density. The former increases the time spent assembling and inverting the Kriging matrices, while the latter increases the time spent searching for the nearest GPs and Master Element. It is also clear that the Planar method scales comparably to IVR, while the Master-Slave differs only slightly with the increase of GPs. Comparing Planar and Master-Slave selection methods, the critical difference is due to the non-linear increase of the time taken assessing the local neighbourhood, and assembling and inverting the Kriging matrix. Albeit a small increase, its effects stack due to the high number of GPs.

The average number of GPs used in each evaluation for the Master-Slave method can be estimated by dividing the target GPs into two groups: internal and surface located GPs (the number of GPs on the edges is negligible). Each GP in the former group has 27 donor GPs available to define the domain, while the latter only has 18 GPs. Thus, the average dimension of the system is 22.5, compared to the average of 9 for the Planar method. This can explain the additional increase of the computational time with the increase of target GPs to be evaluated, obtained for the Master-Slave method when compared with the Planar method.

4. Trimming example

The second example considers a trimming operation, performed on a rectangular specimen that was submitted to a bending operation. This example is selected because it leads to a through-thickness stress gradient similar to the ones that occur in sheet metal forming operations. The springback prediction, which is one of the main sources of geometrical and dimensional inaccuracy in sheet metal formed components, is known to be very sensitive to the accurate evaluation of this gradient (e.g. Refs. [42,43]). Thus, in processes involving trimming operations, it is important to minimize the impact of the remapping in its evaluation. The rectangular specimen has a length of 20 mm (40 elements), width of 5 mm (10 elements) and a thickness of 1 mm (2 elements). It is constrained on one side and symmetry conditions are applied on both lateral faces, while a displacement of 10 mm is applied on the free end, as shown in Fig. 11. After this bending operation (before springback), the specimen is cut by the plane presented in Fig. 11. The geometrical trimming operation was performed with DD3TRIM, using a correction method for the trimmed elements that relocates the nodes associated with the trimmed elements onto the trimming surface [18,40]. After the trimming process, the remapping of the state variables was performed only on the elements modified by this operation (total of 146 GPs). The results for the von Mises equivalent stress are shown in Fig. 12, comparing the distribution before and after trimming.

Concerning the upper surface of the specimen shown in Fig. 12, only negligible changes are induced by the remapping operation, whatever the method adopted. Furthermore, all methods display similar distributions along the thickness. There is no analytical result for direct comparison and the adoption of a more refined mesh as reference solution would generate GPs located in different positions, making the direct comparison between state variable impossible. Hence, based on the results of the previous example, the results obtained with the Planar selection method were used as a baseline for comparison. The relative error *ER* is defined as:

$$ER = \frac{\alpha^{\text{Method}}(\mathbf{x}_t) - \alpha^{\text{Planar}}(\mathbf{x}_t)}{\alpha^{\text{Planar}}(\mathbf{x}_t)}. \tag{11}$$

where α^{Planar} is the value interpolated by the Planar method, in a given target GP with Cartesian coordinates $\mathbf{x}_t$, and α^{Method} is the value obtained

Fig. 11. Schematic representation of the specimen configuration after the bending operation, including the trimming plane.

by either the IVR or the Master-Slave method, in the same GP.

Fig. 13 presents the histogram of the relative error for the trimming example. Both the IVR and the Master-Slave methods provide results that tend to deviate from the ones obtained with the Planar method. As shown in Fig. 12, as expected, the equivalent stress decreases along the length of the specimen (from the fixed support), and from the exterior to the interior (along the thickness direction). Both IVR and Master-Slave methods consider the influence of the GPs that are located near the external surfaces and, consequently, attain slightly higher values for the interior GPs than the Planar method. Therefore, the histogram presents more occurrences on the positive side of the axis (see Equation (11)).

The difference between the maximum values given by IVR and Master-Slave is about 1.2%. A total of 113 and 97 GPs are within the 1% range; and 141 and 139 GPs are within the 2% range, respectively for IVR and Master-Slave. At 2.5%, both methods have 144 GPs; the remaining two GPs appear between 2.5% and 3% for the IVR method, and 4% and 4.5% for the Master-Slave. All methods provide good overall results, and thus, can be used in conjunction with a trimming algorithm.

Table 8 shows the computational time obtained for the remapping tests, showing that both Dual Kriging interpolation methods can lead to a quarter of IVR's computational time. The difference between Master-Slave and Planar is small for this case; but, as shown in the previous section, it will increase with the number of GPs that require remapping, i.e. 2% is insignificant for most applications but will become relevant if applied multiple times. Based on other validation tests, the relative proportions will not change significantly (up to 5%). These computational time results are representative of the time for adaptive mesh refinement algorithms, where no complex search algorithms are required due to the availability of the information regarding the equivalence between old and new finite elements.

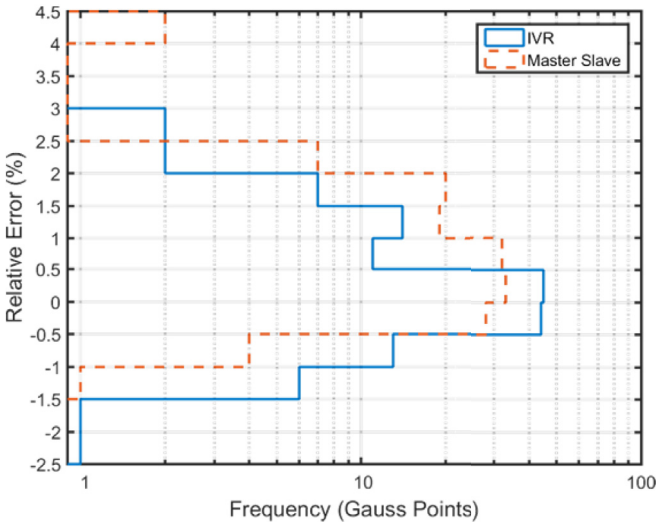

Fig. 13. Histograms of the relative error in the remapping of the equivalent stress obtained in the bending test, after the trimming operation (total of 146 target GPs).

Table 8
Computational time (seconds) and relative difference of the Dual Kriging methods to IVR: Trimming Example.

	IVR ($nl = 5$)	Master-Slave	Planar
Remapping Step	4.47	1.13 (25.2%)	1.06 (23.7%)

Average time for 12 executions on an i7-4860HQ 2.40–3.20 GHz, always discarding two extreme values. Values rounded.

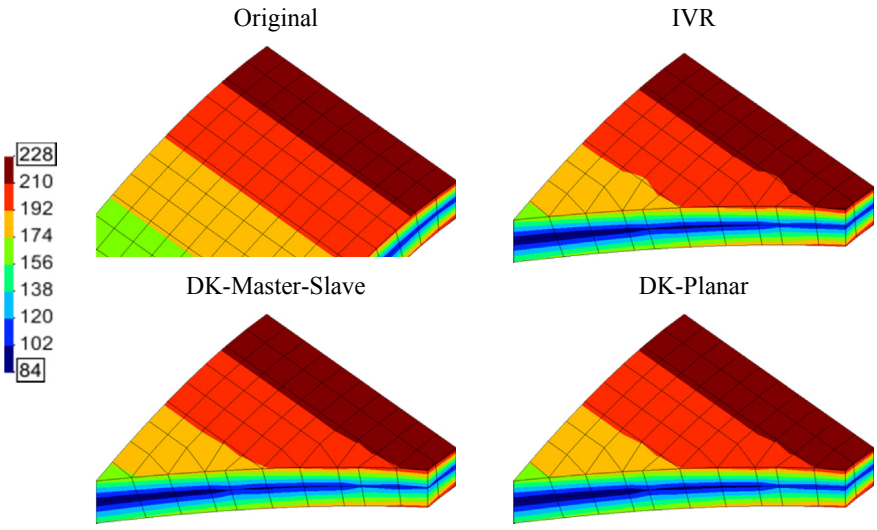

Fig. 12. Distribution of the equivalent stress after the bending operation (Original) and after the trimming operation, as obtained with the Incremental Volumetric Remapping (IVR), Dual Kriging Master-Slave and Planar Dual Kriging.

5. Conclusions

This work presents the application of the Dual Kriging interpolation method as remapping scheme for FEM state variables between different finite element meshes. Only the standard 8-node hexahedral finite elements are addressed, considering the state variable assigned to the Gauss Points. Since both the computational cost and the accuracy of the Dual Kriging method is influenced by the amount of information used, two different selection algorithms were developed, namely the Master-Slave and Planar. Additionally, the developed remapping method is compared with the IVR method, both in terms of accuracy and computational performance.

For the examples considered in the present study, all remapping methods can provide results with a good level of accuracy. The first example dealt with the remapping of an analytical function between finite element meshes of different topologies. Assuming there is no gradient of the variable along one direction, the Master-Slave and Planar methods present a significant improvement over the IVR. When considering a state variable distribution with gradient in all directions, combined with a small thickness dimension, a decrease of accuracy is observed for the Master-Slave method, due to an overweighting of the through-thickness component, while the Planar method kept its level of accuracy. Nevertheless, it should be mentioned that the accuracy of the IVR method can be improved, increasing the value of the *nl* parameter, which also results in an increase of the computational time. Regarding this topic, the computational cost incurred for the Dual Kriging method is lower than the one obtained with the IVR, particularly for related meshes, such as the ones used in remapping after trimming or remeshing.

Acknowledgements

The authors gratefully acknowledge the financial support of the Portuguese Foundation for Science and Technology (FCT) under projects P2020-PTDC/EMS-TEC/0702/2014 (POCI-01-0145-FEDER-016779) and P2020-PTDC/EMS-TEC/6400/2014 (POCI-01-0145-FEDER-016876) by UE/FEDER through the program COMPETE 2020. The second author is also grateful to the FCT for the Postdoctoral grant SFRH/BPD/101334/2014.

References

[1] V. Thomée, From finite differences to finite elements: a short history of numerical analysis of partial differential equations, J. Comput. Appl. Math. 128 (2001) 1–54, https://doi.org/10.1016/S0377-0427(00)00507-0.
[2] K.K. Gupta, J.L. Meek, A brief history of the beginning of the finite element method, Int. J. Numer. Methods Eng. 39 (1996) 3761–3774, https://doi.org/10.1002/(SICI)1097-0207(19961130)39:22<3761::AID-NME22>3.0.CO;2–5.
[3] C. Veyhl, I.V. Belova, G.E. Murch, A. Öchsner, T. Fiedler, On the mesh dependence of non-linear mechanical finite element analysis, Finite Elem. Anal. Des. 46 (2010) 371–378, https://doi.org/10.1016/j.finel.2009.12.003.
[4] O.C. Zienkiewicz, R.L. Taylor, The Finite Element Method for Solid and Structural Mechanics, Elsevier Butterworth-Heinemann, 2005.
[5] K. Suresh, S.P. Regalla, Effect of mesh parameters in finite element simulation of single point incremental sheet forming process, Proced. Mater. Sci. 6 (2014) 376–382, https://doi.org/10.1016/j.mspro.2014.07.048.
[6] M.A. Shayanfar, A. Kheyroddin, M.S. Mirza, Element size effects in nonlinear analysis of reinforced concrete members, Comput. Struct. 62 (1997) 339–352, https://doi.org/10.1016/S0045-7949(96)00007-7.
[7] S. Andrietti, J.-L. Chenot, M. Bernacki, P.-O. Bouchard, L. Fourment, E. Hachem, E. Perchat, Recent and future developments in finite element metal forming simulation, Comput. Methods Mater. Sci. 15 (2015) 265–293.
[8] M. Schäer, Computational Engineering: Introduction to Numerical Methods, Springer, 2006.
[9] S.W. Chung, S.J. Kim, A remeshing algorithm based on bubble packing method and its application to large deformation problems, Finite Elem. Anal. Des. 39 (2003) 301–324, https://doi.org/10.1016/S0168-874X(02)00075-6.
[10] B. Lu, H. Ou, An efficient approach for trimming simulation of 3D forged components, Int. J. Mech. Sci. 55 (2012) 30–41, https://doi.org/10.1016/j.ijmecsci.2011.11.013.
[11] P. Bussetta, R. Boman, J.-P. Ponthot, Efficient 3D data transfer operators based on numerical integration, Int. J. Numer. Methods Eng. 102 (2015) 892–929, https://doi.org/10.1002/nme.4821.
[12] M. Bambach, Fast simulation of incremental sheet metal forming by adaptive remeshing and subcycling, Int. J. Mater. Form. 9 (2016) 353–360, https://doi.org/10.1007/s12289-014-1204-9.
[13] R.D. Russell, Adaptive mesh refinement, in: Encycl. Appl. Comput. Math., Springer Berlin Heidelberg, Berlin, Heidelberg, 2015, pp. 23–25, https://doi.org/10.1007/978-3-540-70529-1_341.
[14] X. Jiao, M.T. Heath, Common-refinement-based data transfer between non-matching meshes in multiphysics simulations, Int. J. Numer. Methods Eng. 61 (2004) 2402–2427, https://doi.org/10.1002/nme.1147.
[15] M.M. Rashid, Material state remapping in computational solid mechanics, Int. J. Numer. Methods Eng. 55 (2002) 431–450, https://doi.org/10.1002/nme.508.
[16] E. Hinton, J.S. Campbell, Local and global smoothing of discontinuous finite element functions using a least squares method, Int. J. Numer. Methods Eng. 8 (1974) 461–480, https://doi.org/10.1002/nme.1620080303.
[17] D. Perić, C. Hochard, M. Dutko, D.R.J. Owen, Transfer operators for evolving meshes in small strain elasto-plasticity, Comput. Methods Appl. Mech. Eng. 137 (1996) 331–344, https://doi.org/10.1016/S0045-7825(96)01070-5.
[18] A.J. Baptista, Mechanical Modelling and Numerical Simulation of the Multi-step Sheet Metal Forming Process, University of Coimbra, 2006.
[19] M.L. Alves, J.L.M. Fernandes, J.M.C. Rodrigues, P.A.F. Martins, Finite element remeshing in metal forming using hexahedral elements, J. Mater. Process. Technol. 141 (2003) 395–403, https://doi.org/10.1016/S0924-0136(03)00388-1.
[20] O.C. Zienkiewicz, J.Z. Zhu, The superconvergent patch recovery (SPR) and adaptive finite element refinement, Comput. Methods Appl. Mech. Eng. 101 (1992) 207–224, https://doi.org/10.1016/0045-7825(92)90023-D.
[21] D.-Y. Kwak, Y.-T. Im, Remeshing for metal forming simulations-Part II: three-dimensional hexahedral mesh generation, Int. J. Numer. Methods Eng. 53 (2002) 2501–2528, https://doi.org/10.1002/nme.404.
[22] L.G. Margolin, M. Shashkov, Second-order sign-preserving conservative interpolation (remapping) on general grids, J. Comput. Phys. 184 (2003) 266–298, https://doi.org/10.1016/S0021-9991(02)00033-5.
[23] C. Farhat, M. Lesoinne, P. Le Tallec, Load and motion transfer algorithms for fluid/structure interaction problems with non-matching discrete interfaces: momentum and energy conservation, optimal discretization and application to aeroelasticity, Comput. Methods Appl. Mech. Eng. 157 (1998) 95–114, https://doi.org/10.1016/S0045-7825(97)00216-8.
[24] R. Luce, M. Wolske, R. Kopp, F. Roters, G. Gottstein, Application of a dislocation model for FE-process simulation, Comput. Mater. Sci. 21 (2001) 1–8, https://doi.org/10.1016/S0927-0256(00)00210-X.
[25] M. Ortiz, J.J. Quigley, Adaptive mesh refinement in strain localization problems, Comput. Methods Appl. Mech. Eng. 90 (1991) 781–804, https://doi.org/10.1016/0045-7825(91)90184-8.
[26] J.K. Dukowicz, J.R. Baumgardner, Incremental remapping as a transport/advection algorithm, J. Comput. Phys. 160 (2000) 318–335, https://doi.org/10.1006/jcph.2000.6465.
[27] P. Bochev, M. Shashkov, Constrained interpolation (remap) of divergence-free fields, Comput. Methods Appl. Mech. Eng. 194 (2005) 511–530, https://doi.org/10.1016/j.cma.2004.05.018.
[28] T.J.R. Hughes, Generalization of selective integration procedures to anisotropic and nonlinear media, Int. J. Numer. Methods Eng. 15 (1980) 1413–1418, https://doi.org/10.1002/nme.1620150914.
[29] A.J. Baptista, J.L. Alves, M.C. Oliveira, D.M. Rodrigues, L.F. Menezes, Incremental volumetric remapping method: analysis and error evaluation, in: AIP Conf. Proc., AIP, 2007, pp. 835–840, https://doi.org/10.1063/1.2740914.
[30] A.J. Baptista, J.L. Alves, M.C. Oliveira, D.M. Rodrigues, L.F. Menezes, Application of the incremental volumetric remapping method in the simulation of multi-step deep drawing processes, in: AIP Conf. Proc., AIP, 2005, pp. 173–178, https://doi.org/10.1063/1.2011213.
[31] P. McLean, P. Léger, R. Tinawi, Post-processing of finite element stress fields using dual kriging based methods for structural analysis of concrete dams, Finite Elem. Anal. Des. 42 (2006) 532–546, https://doi.org/10.1016/j.finel.2005.10.004.
[32] J. Grandy, Conservative remapping and region overlays by intersecting arbitrary polyhedra, J. Comput. Phys. 148 (1999) 433–466, https://doi.org/10.1006/jcph.1998.6125.
[33] D.G. Krige, A review of the development of geostatistics in South Africa, in: Adv. Geostatistics Min. Ind., Springer Netherlands, Dordrecht, 1976, pp. 279–293, https://doi.org/10.1007/978-94-010-1470-0_17.
[34] G. Matheron, Les Concepts de Base et L'Evolution de la Geostatistique Miniere, in: Adv. Geostatistics Min. Ind., Springer Netherlands, Dordrecht, 1976, pp. 3–10, https://doi.org/10.1007/978-94-010-1470-0_1.
[35] C. Poirier, R. Tinawi, Finite element stress tensor fields interpolation and manipulation using 3D dual kriging, Comput. Struct. 40 (1991) 211–222, https://doi.org/10.1016/0045-7949(91)90348-P.
[36] F. Trochu, A contouring program based on dual kriging interpolation, Eng. Comput. 9 (1993) 160–177, https://doi.org/10.1007/BF01206346.
[37] D.J.J. Toal, A study into the potential of GPUs for the efficient construction and evaluation of Kriging models, Eng. Comput. 32 (2016) 377–404, https://doi.org/10.1007/s00366-015-0421-2.
[38] E. Anderson, Z. Bai, C. Bischof, S. Blackford, J. Demmel, J. Dongarra, J. Du Croz, A. Greenbaum, S. Hammarling, A. McKenney, D. Sorensen, LAPACK Users' Guide,

Society for Industrial and Applied Mathematics, 1999. http://www.netlib.org/lapack/lug/. (Accessed 12 April 2017).
[39] C.M.A. Diogo, DD3TRIM - Revised and Augmented Version, University of Coimbra, 2015.
[40] A.J. Baptista, J.L. Alves, D.M. Rodrigues, L.F. Menezes, Trimming of 3D solid finite element meshes using parametric surfaces: application to sheet metal forming, Finite Elem. Anal. Des. 42 (2006) 1053–1060, https://doi.org/10.1016/j.finel.2006.03.005.
[41] A. Coll, R. Ribó, M. Pasenau, E. Escolano, J. Perez, GiD v. 13 Reference Manual, 2016.
[42] K.P. Li, W.P. Carden, R.H. Wagoner, Simulation of springback, Int. J. Mech. Sci. 44 (2002) 103–122, https://doi.org/10.1016/S0020-7403(01)00083-2.
[43] T. Meinders, I.A. Burchitz, M.H.A. Bonte, R.A. Lingbeek, Numerical product design: springback prediction, compensation and optimization, Int. J. Mach. Tools Manuf. 48 (2008) 499–514, https://doi.org/10.1016/j.ijmachtools.2007.08.006.